JOURNAL OF GUIDANCE, CONTROL, AND DYNAMICS
Vol. 30, No. 4, July–August 2007

Engineering Notes

ENGINEERING NOTES are short manuscripts describing new developments or important results of a preliminary nature. These Notes should not exceed 2500 words (where a figure or table counts as 200 words). Following informal review by the Editors, they may be published within a few months of the date of receipt. Style requirements are the same as for regular contributions (see inside back cover).

Three-Dimensional Aircraft Terrain-Following via Real-Time Optimal Control

Paul Williams*
Royal Melbourne Institute of Technology University, Bundoora, Victoria 3083, Australia

DOI: 10.2514/1.29145

I. Introduction

THE determination of optimal aircraft trajectories has been of considerable interest to aircraft dynamicists for almost 50 years. The complexity of aircraft dynamics, in general, requires the separation of the guidance and control design into inner and outer loops. The outer loop is driven by the navigation requirements. Typically, aircraft point-mass models are used for aircraft trajectory optimization when some aircraft performance parameters, such as lift, drag, and thrust need to be calculated. Other approaches that have been used for aircraft navigation around terrain and obstacles are often based only on kinematic considerations.

It is well recognized that terrain-following trajectories are important for many military aircraft in defense applications [1]. Menon et al. [2] developed a kinematic approach for determining optimal terrain-following flight by explicitly incorporating the terrain profile into the kinematics. The extension of this work to incorporate moving threats and targets has recently been presented by Twigg et al. [3]. Richards and How [4] considered planar motion for aircraft trajectory planning for avoiding obstacles using a simplified aircraft model moving at constant velocity. Xu et al. [5] considered terrain-following control using a backstepping controller designed to track a commanded angle of attack. Funk [6] considered terrain following under the requirements that the aircraft lie as close as possible to all the terrain points and that the trajectory be capable of being accurately followed by the aircraft. Solutions were generated by parameterizing the aircraft altitude using cubic splines whose parameters were determined by solving a nonlinear programming problem. Combined terrain following/avoidance was considered by Asseo [7] who used a steepest descent method to optimize the lateral motion of the aircraft, and parabolic flight segments for the longitudinal motion to clear the critical terrain points. The longitudinal aircraft dynamics of a point-mass aircraft were incorporated into the optimization problem by Lu and Pierson [8], who also considered trajectory tracking via predictive control [9]. In most of these studies, the performance index is selected as a weighted minimum time and minimum altitude (quadratic) criterion. Williams [10] used a pseudospectral method combined with global polynomials to obtain constrained optimal trajectories incorporating the aircraft control actuators. Sharma et al. [11] used direct transcription to obtain minimax optimal terrain-following trajectories, and used a receding horizon control strategy to obtain closed-loop trajectories for a point-mass aircraft model assuming errors in aerodynamic coefficients. A cubic B-spline representation of the terrain was used, but computing times were extremely lengthy.

The purpose of this paper is to develop an approach capable of computing optimal aircraft trajectories near terrain in real-time. For this purpose, a suitable analytic representation of three-dimensional terrain is developed using polynomial bases and Kronecker factorization. A three-dimensional point-mass aircraft model is used to obtain the outer-loop optimal trajectories using a Legendre pseudospectral method. A method for converting these trajectories into inner-loop commands, implemented via a receding horizon strategy based on Gauss–Lobatto quadrature rules is also developed, but is not critical to the presentation.

II. Aircraft Dynamic Models

A. Point-Mass Aircraft Model

For the purposes of flight-path control design, it is usually sufficient to treat only the translational motion of the aircraft [12]. In this context, the aircraft angle of attack α and bank angle μ are treated as pseudocontrol inputs, together with the throttle η. The aircraft equations of motion are expressed in a velocity coordinate frame attached to the aircraft. The kinematic equations of the aircraft are given by

$$\dot{x} = V\cos\gamma\cos\chi + W_x \qquad \dot{y} = V\cos\gamma\sin\chi + W_y$$
$$\dot{z} = V\sin\gamma + W_z \tag{1}$$

where V is the aircraft velocity relative to the wind, γ is the flight-path angle, χ is the heading angle, (W_x, W_y, W_z) are components of the wind velocity in the inertial frame, and (x, y, z) are the aircraft inertial coordinates.

The dynamic equations of the aircraft are given by

$$\dot{V} = \frac{T\cos\alpha - D}{m} - g\sin\gamma - \dot{W}_x\cos\gamma\cos\chi - \dot{W}_y\cos\gamma\sin\chi - \dot{W}_z\sin\gamma$$
$$\dot{\chi} = \frac{[L + T\sin\alpha]\sin\phi}{mV\cos\gamma} + \frac{\dot{W}_x\sin\chi}{V\cos\gamma} - \frac{\dot{W}_y\cos\chi}{V\cos\gamma}$$
$$\dot{\gamma} = \frac{[L + T\sin\alpha]\cos\phi}{mV} - \frac{g}{V}\cos\gamma + \frac{\dot{W}_x\sin\gamma\cos\chi}{V} + \frac{\dot{W}_y\sin\gamma\sin\chi}{V} - \frac{\dot{W}_z\cos\gamma}{V} \tag{2}$$

where m is the aircraft mass, $T = \eta T_{\max}$ is the aircraft thrust, $T_{\max}$ is the maximum available thrust, $D = \bar{q}SC_D$ is the drag, g is the acceleration due to gravity, $L = \bar{q}SC_L$ is the lift, $\bar{q} = \rho V^2/2$ is the dynamic pressure, ρ is the air density at the altitude z, and S is the aircraft wing area.

For good numerical scaling, the equations of motion are nondimensionalized by scaling the velocity as $\bar{v} = V/v_s$, and the positions as $\bar{x} = gx/v_s^2$, $\bar{y} = gy/v_s^2$, $\bar{z} = gz/v_s^2$, where v_s is the speed

Received 4 December 2006; revision received 20 January 2007; accepted for publication 23 January 2007.

*Research Fellow, School of Aerospace, Mechanical, and Manufacturing Engineering, P.O. Box 71. AIAA Member.

of sound at sea level. For motion planning near terrain, it is also more convenient to parameterize the trajectories by the downrange (x). Thus, the equations of motion can be expressed in the following nondimensional form:

$$\frac{\mathrm{d}\bar{y}}{\mathrm{d}\bar{x}} = \frac{\bar{v}\cos\gamma\sin\chi + W_y/v_s}{\bar{v}\cos\gamma\cos\chi + W_x/v_s} \tag{3}$$

$$\frac{\mathrm{d}\bar{z}}{\mathrm{d}\bar{x}} = \frac{\bar{v}\sin\gamma + W_z/v_s}{\bar{v}\cos\gamma\cos\chi + W_x/v_s} \tag{4}$$

$$\frac{\mathrm{d}\bar{v}}{\mathrm{d}\bar{x}} = \left(\frac{T\cos\alpha - D}{m} - g\sin\gamma - \dot{W}_x\cos\gamma\cos\chi - \dot{W}_y\cos\gamma\sin\chi - \dot{W}_z\sin\gamma\right)\frac{1}{g(\bar{v}\cos\gamma\cos\chi + W_x/v_s)} \tag{5}$$

$$\frac{\mathrm{d}\chi}{\mathrm{d}\bar{x}} = \left(\frac{[L + T\sin\alpha]\sin\mu}{m\bar{v}\cos\gamma} + \frac{\dot{W}_x\sin\chi}{\bar{v}\cos\gamma} - \frac{\dot{W}_y\cos\chi}{\bar{v}\cos\gamma}\right)\frac{1}{g(\bar{v}\cos\gamma\cos\chi + W_x/v_s)} \tag{6}$$

$$\frac{\mathrm{d}\gamma}{\mathrm{d}\bar{x}} = \left(\frac{[L + T\sin\alpha]\cos\mu}{m\bar{v}} - \frac{g}{\bar{v}}\cos\gamma + \frac{\dot{W}_x\sin\gamma\cos\chi}{\bar{v}} + \frac{\dot{W}_y\sin\gamma\sin\chi}{\bar{v}} - \frac{\dot{W}_z\cos\gamma}{\bar{v}}\right)\frac{1}{g(\bar{v}\cos\gamma\cos\chi + W_x/v_s)} \tag{7}$$

Thus, the parameterization becomes more physically meaningful because it is easier to set a future downrange position than it is to set a future time. To these equations must be added an equation that relates the downrange to time because this must ultimately be used to fly the trajectories

$$\frac{\mathrm{d}t}{\mathrm{d}\bar{x}} = \frac{1}{\bar{v}\cos\gamma\cos\chi + W_x/v_s}\left(\frac{v_s}{g}\right) \tag{8}$$

Note that any linear factor can also be used to scale Eq. (8) because the physical time is a much larger quantity than the nondimensional variables. One of the limitations of the equations of motion in this form is that it does not easily allow 90 deg turns. This would necessitate reinitializing the downrange to maintain a monotonic variation in the independent variable. This, however, is not a problem for the types of terrain-following trajectories being considered here.

1. Aerodynamic Data

In this paper, the specific aircraft considered is the F-4 Phantom. The aerodynamic data are taken from the six-degree-of-freedom aircraft model to be described later. The lift and drag coefficients are nonlinearly dependent on the angle of attack α according to

$$C_L = (-0.0434 + 0.1369\alpha)\sin\alpha + (0.131 + 3.0825\alpha)\cos\alpha \tag{9}$$

$$C_D = (0.0434 - 0.1369\alpha)\cos\alpha + (0.131 + 3.0825\alpha)\sin\alpha \tag{10}$$

which are valid for angles of attack $\alpha \leq 15$ deg.

2. Thrust Data

Thrust data for the F-4 aircraft were taken from data originally presented in [13], and also available in [14]. The maximum available thrust is expressed in units of 1000 lb, and is a function of the Mach number $\bar{v}$ and altitude h in units of 10,000 ft,

$$T_{\max} = [1, \bar{v}, \bar{v}^2, \bar{v}^3, \bar{v}^4]\begin{bmatrix} 30.21 & -0.668 & -6.877 & 1.951 & -0.1512 \\ -33.80 & 3.347 & 18.13 & -5.865 & 0.4757 \\ 100.80 & -77.56 & 5.441 & 2.864 & -0.3355 \\ -78.99 & 101.40 & -30.28 & 3.236 & -0.1089 \\ 18.74 & -31.60 & 12.04 & -1.785 & 0.09417 \end{bmatrix}\times\begin{bmatrix} 1 \\ h \\ h^2 \\ h^3 \\ h^4 \end{bmatrix} \tag{11}$$

B. Six-Degree-of-Freedom Aircraft Model

To more accurately simulate the flight of the optimal trajectories, a more accurate aircraft model that treats both the translational and rotational motion is considered. For simplicity, only the rigid body motion of the aircraft is treated here. The dynamic force equations are recast in terms of the derivatives of the airspeed, angle of attack, and sideslip angle. Winds are incorporated into the model such that the angle of attack, sideslip, and airspeed are measured relatively to the wind. The winds are specified in the inertial coordinate system, and are transformed into the aircraft body frame using standard transformations [15]. The full equations of motion and aerodynamic data are omitted for the sake of brevity. The reader is referred to [16] for more details.

C. Terrain Model

As mentioned previously, to compute trajectories in speeds approaching real time, it is necessary to employ a terrain representation that allows quick computations of local terrain height as well as derivatives of the terrain. Here, it is assumed that the local terrain data are available in the form of gridded data. This could be measured in flight or available in a terrain database. The precise mechanism for obtaining the terrain data is not the main issue here. The terrain data are fitted using a two variable polynomial as

$$z_T(\bar{x}, \bar{y}) = \sum_{i=0}^{n_x}\sum_{j=0}^{n_y} c_{i,j}[\tilde{x}(\bar{x})]^i[\tilde{y}(\bar{y})]^j \tag{12}$$

where the $(\tilde{x}, \tilde{y})$ coordinates are scaled to be between -1 and 1 according to the transformation

$$\tilde{x}(\bar{x}) = \frac{2\bar{x} - \bar{x}_{\max} - \bar{x}_{\min}}{(\bar{x}_{\max} - \bar{x}_{\min})} \tag{13}$$

and similar for $\tilde{y}$. It is straightforward to express the terrain height as a function of the original downrange and cross range, but this form retains better scaling. The terrain data are fitted using a least-squares solution. The vector of terrain data can be written as

$$z = [H]\boldsymbol{c} \tag{14}$$

where H is expressed as a Kronecker factorization of two Vandermonde matrices H_x and H_y

$$H \triangleq H_x \otimes H_y \tag{15}$$

The least-squares solution for the $\boldsymbol{c}$ vector is given by

$$\boldsymbol{c} = \left\{\left[\left(H_x^T H_x\right)^{-1} H_x^T\right] \otimes \left[\left(H_y^T H_y\right)^{-1} H_y^T\right]\right\} z \tag{16}$$

Using this model, it is easy to compute derivatives with respect to the aircraft position. For example, derivatives with respect to the nondimensional y coordinate can be calculated according to (using

the chain rule)

$$\frac{\mathrm{d}z_T(\bar{x},\bar{y})}{\mathrm{d}\bar{y}} = \frac{2}{\bar{y}_{\max}-\bar{y}_{\min}}\sum_{i=0}^{n_x}\sum_{j=1}^{n_y} jc_{i,j}\tilde{x}^i\tilde{y}^{j-1} \tag{17}$$

III. Real-Time Optimal Control Using Legendre Pseudospectral Method

A. Outer-Loop Guidance Formulation

Consider the problem of finding the optimal state trajectory $\boldsymbol{x}(\bar{x}) = [\bar{y}, \bar{z}, \bar{v}, \gamma, \chi, t]^T$, and the corresponding control input $\boldsymbol{u}(\bar{x}) = [\eta, \alpha, \mu]^T$ such that the cost function

$$J = \int_{x_0}^{x_f}\left[W_1\bar{v}'^2 + W_2\gamma'^2 + W_3\chi'^2 + W_4(z-z_T)^2\right]\mathrm{d}\bar{x} \tag{18}$$

is minimized, where W_1, W_2, W_3, W_4 are constant weighting coefficients. This cost trades the acceleration and flight-path angular rates with the terrain-following capability. The first three terms tend to smooth the trajectory and associated pseudocontrol inputs. This cost is subject to the dynamic equations given by Eqs. (3–8), as well as the following path constraints

$$z - z_T \geq 50 \text{ m} \tag{19}$$

$$0.1 \leq \bar{v} \leq 0.95 \tag{20}$$

$$0 \leq \eta \leq 1 \tag{21}$$

$$-2 \leq \alpha \leq 15 \text{ deg} \tag{22}$$

$$-60 \leq \mu \leq 60 \text{ deg} \tag{23}$$

Initial conditions constraints are also enforced, but the terminal boundary conditions are free.

The solution to the preceding problem is obtained using the Legendre pseudospectral method [17,18]. This approach has been selected because it is very easy to compute analytic Jacobians for the discretized conditions. Essentially, the states and controls are expanded based on Lagrange interpolating polynomials using values of the states and controls at the Legendre–Gauss–Lobatto points as coefficients. This enables state and control constraints to be easily incorporated into the problem. The approach transforms the continuous optimal control problem into a discrete parameter optimization problem. The resulting nonlinear programming problem is solved using the software SNOPT [19].

B. Inner-Loop Tracker Using Linear Receding Horizon Strategy

The generation of optimal outer-loop trajectories (i.e., positions, velocities, angle of attack, and bank angle) can be achieved using the methodology previously outlined. However, to implement it in the six-degree-of-freedom model requires some additional computations and feedback. Essentially, the flight-path angles and pseudocontrols are used to convert the outer-loop trajectory into body axis angular velocities and angular accelerations. This can be achieved by using the direction cosine matrix that relates the body frame to the inertial frame to obtain the quaternion representation of the aircraft attitude. The result is differentiated with respect to time by either fitting cubic splines to the quaternions or using the differentiation matrix that is used in the Legendre pseudospectral method. The required moments are then computed from the aircraft moment equations, and the required control deflections are obtained by solving the simultaneous equations. Explicit details of this process are given in [16]. The actual moment coefficients used for the F-4 contain several nonlinear terms, which are neglected in the computation of the actuator reference profiles. The resulting changes in aerodynamics of the vehicle are also neglected. For implementation, the actuator signals are computed from first-order differential equations to maintain continuity in the actuator deflections.

Using the reference angle of attack, throttle, and actuator profiles, the equations of motion of the aircraft are linearized around the time-varying reference trajectories. This includes all translational and moment equations. The result may be expressed as

$$\delta\dot{\boldsymbol{x}}(t) = [\boldsymbol{A}(t)]\delta\boldsymbol{x}(t) + [\boldsymbol{B}(t)]\delta\boldsymbol{u}(t) \tag{24}$$

where $\boldsymbol{A} \in \mathbb{R}^{n\times n}$ is the time-varying state influence matrix, and $\boldsymbol{B} \in \mathbb{R}^{n\times m}$ is the time-varying control influence matrix. The perturbed controls $\delta\boldsymbol{u}(t)$ for tracking the reference trajectories are found so as to minimize the performance index

$$J = \frac{1}{2}\int_t^{t+T}\left[\delta\boldsymbol{x}^\top(t^*)\boldsymbol{Q}\delta\boldsymbol{x}(t^*) + \delta\boldsymbol{u}^\top(t^*)\boldsymbol{R}\delta\boldsymbol{x}(t)\right]\mathrm{d}t^* \tag{25}$$

where $\boldsymbol{Q} \in \mathbb{R}^{n\times n}$ is a positive-semidefinite weighting matrix for the penalizing deviations of the states from their reference values, and $\boldsymbol{R} \in \mathbb{R}^{m\times m}$ is a positive-definite weighting matrix for the penalizing deviations of the controls from their reference values. Equation (25) is subject to the perturbed state equations [Eq. (24)], the initial conditions

$$\delta\boldsymbol{x}(t) = \boldsymbol{x}(t) - \bar{\boldsymbol{x}}(t) \tag{26}$$

and terminal constraints

$$\delta\boldsymbol{x}(t+T) = \boldsymbol{0} \tag{27}$$

where $\bar{\boldsymbol{x}}(t) = [x, y, z, \bar{v}, \alpha, \beta, \phi, \theta, \psi, p, q, r, \delta_E, \delta_A, \delta_R]^T$ is the reference trajectory evaluated at the current time, and $\boldsymbol{u}(t) = [\eta, \dot{\delta}_E, \dot{\delta}_A, \dot{\delta}_R]$.

This receding horizon control problem can be solved using numerical integration of the Riccati equation. However, this can be quite time-consuming and tedious to formulate. It can also suffer from numerical instabilities. Instead, a method based on Gauss–Lobatto quadrature is used to generate the optimal time-varying feedback gains in an efficient and robust manner. The approach is based in part on the method and references in [20] and is outlined in detail in [21]. Essentially, the feedback control is expressed in the form

$$\delta\boldsymbol{u}(t) = \boldsymbol{K}(t)\delta\boldsymbol{x}(t) \tag{28}$$

where $\boldsymbol{K}(t) \in \mathbb{R}^{m\times n}$ is the optimal time-varying feedback gain matrix.

IV. Numerical Results

Closed-loop simulations were performed using the preceding techniques with a future horizon length of 5 km and $N = 16$ for the nonlinear trajectory updates. This level of discretization was selected to give the best combination of speed and accuracy. The sampling time is set as 2.5 s and the weighting matrices for the feedback controller are selected as

$$\boldsymbol{Q} = \mathrm{diag}[1, 1, 1, 100, 100, 100, 1, 10000, 100, 100, 100, 100] \tag{29}$$

$$\boldsymbol{R} = \mathrm{diag}[10000, 1000, 1000, 1000] \tag{30}$$

For actual implementation, the initial pseudocontrols and throttle are constrained to be equal to the actual angle of attack, bank angle, and throttle from the closed-loop simulation. This ensures that there are no sudden jumps in the pseudocontrols, which would inevitably lead to jumps in the reference trajectories and make the system more difficult to track. Disturbances are applied to the closed-loop simulation that are not applied in the reference model. For example, the aerodynamics of the aircraft is naturally different due to the

Table 1 Summary of Monte Carlo results over 100 runs, showing differences between steady winds and random unsteady winds

Parameter	Average mean difference	Average min. difference	Average max. difference	Average standard deviation of difference
Roll, deg	0.393	−10.689	12.134	4.172
Pitch, deg	0.186	−2.234	3.227	0.896
Yaw, deg	0.076	−3.059	3.509	1.587
Mach no.	−0.0098	−0.019	0.0018	0.005
Alpha, deg	0.219	−1.815	2.641	0.539
Sideslip, deg	0.013	−0.618	0.910	0.198
Elevator, deg	−0.089	−1.695	1.625	0.308
Ailerons, deg	−0.0006	−3.955	4.476	1.097
Rudder, deg	0.0433	−1.593	2.120	0.545
Throttle	−0.010	−0.110	0.103	0.038
Height above terrain, m[a]	235.49	44.76 (global min. 37.87)	543.83 (global max. 719.11)	150.01

[a]Note that height above terrain is shown in an absolute sense and is not relative to the steady winds case.

effects of actuator deflections. The most important disturbance is due to the effects of winds. In the closed-loop simulation, unsteady winds in the x and y directions are applied with a means of 2 and 10 m/s, respectively, and standard deviation of 2.5 m/s. The winds are assumed to be constant between updates, but this information is unavailable to the trajectory generation algorithm. It is important to realize that when the aircraft operates close to the minimum height above terrain constraint, a disturbance between samples could cause the aircraft to fall below the constraint. This causes the trajectory update to fail because the path constraint cannot be satisfied. Therefore, at each new sample, the estimated height above the terrain is used to test the constraint before the trajectory update. If the constraint is violated, the minimum height above the terrain is decreased by the amount of violation plus an additional 10% to enable a feasible solution. The decrease in the constraint is used only when the aircraft is initially violating the constraint and is returned to the desired value immediately after the sample.

Monte Carlo closed-loop simulations were performed from the same initial conditions of $[x(0), y(0), z(0), \bar{v}(0), \gamma(0), \chi(0)] = [-9000\ \text{m}, -1000\ \text{m}, 400\ \text{m}, 0.5, 0, 0]$. For reference, the aircraft mass is assumed to be $m = 19,050$ kg, the wing area is $S = 49.2\ \text{m}^2$, $I_{xx} = 33,854.76\ \text{kg} \cdot \text{m}^2$, $I_{yy} = 165,667.32\ \text{kg} \cdot \text{m}^2$, $I_{zz} = 189,543.27\ \text{kg} \cdot \text{m}^2$, $\bar{c} = 4.8768$ m, and $b = 11.796$ m. The atmospheric density is assumed to follow the International Standard Atmosphere. The terrain was generated using a terrain generation algorithm. For the purposes of comparison, the differences between the closed-loop simulation conducted with steady winds and unsteady winds is made. Monte Carlo simulations using 100 different random seeds were carried out. All solutions were generated using a Centrino Duo T2600 2.16 GHz processor. Because of the amount of data produced, only a selection of results is shown in the following figures. The remaining data are summarized in Table 1. Figure 1 shows the three-dimensional terrain together with a random sample of 25 closed-loop trajectories. The results illustrate that the aircraft tends to be guided in relatively the same path in the presence of disturbances. The trajectory can be seen to vary in both altitude and cross range. Figure 2 shows a selection of the aircraft airflow angles together with the corresponding control actuator inputs. The results indicate that the closed-loop trajectories tend to be much smoother in the case of steady winds compared with the case of unsteady winds. It is interesting to note that the initial aircraft response and control inputs are similar in all the cases shown. Figure 2a shows that the angle of attack is kept well below the maximum, and the sideslip angle is maintained reasonably well around the desired value of zero. Figures 2b and 2c show the required actuator inputs are also very modest. The mean elevator deflection is approximately −2 deg, with relatively small corrections superimposed (approximately 1 deg in the unsteady case). The maximum aileron deflection is on the order of 5 deg, and the rudder peaks at about 2 deg. Note that the inner-loop design used here is not ideal, and that it is likely that better results can be generated with more robust inner-loop trackers. However, the results show that the aircraft is able to fly successfully without collision. The mean CPU time per update over all runs is 1.002 s (0.235 s standard deviation).

Table 1 gives a statistical summary of the results from the Monte Carlo simulations. The results are summarized relative to the solution generated for the case of steady winds. The idea of this being that the unsteady components of the winds have a mean of zero, so that statistically one would expect the aircraft to stay close to the trajectory generated with steady winds. The average mean difference in the trajectories shown in Table 1 can be seen to be very close to zero, with maximum mean differences occurring for the aircraft roll angle (0.393 deg) and angle of attack (0.219 deg). The mean height of the aircraft above the terrain is 235.49 m, but approaches a minimum, on average, of 44.76 m. Note that this is actually below the path constraint specified by the outer loop. The reason for this is that the disturbances cause the aircraft to drop below the constraint between samples. It is for this reason that it is necessary to reduce the constraint during the next update to allow the trajectory to recover. In the worst case, the aircraft dropped to 37.87 m above the terrain. The columns showing the minimum and maximum differences in Table 1 illustrate that the aircraft operates successfully within the design envelope. Hence, it is evident that combining the outer-loop trajectory generator with a robust inner loop can produce fast optimal trajectories for an aircraft operating close to terrain. Alternative inner loops should be pursued to enhance the quality of the closed-loop trajectories, which would also help to speed up the trajectory updates because the aircraft would be maintained closer to the previous optimal trajectory.

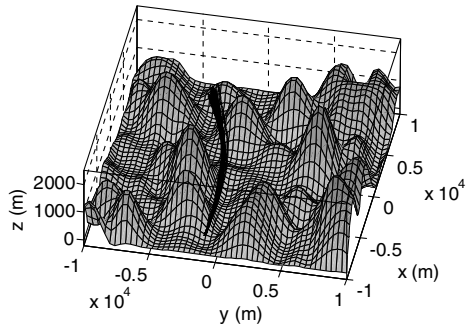

Fig. 1 Dispersions of closed-loop trajectories.

V. Conclusions

Real-time optimal generation of aircraft trajectories is possible for maneuvering in three-dimensions close to terrain using a Legendre pseudospectral method. By using a point-mass model of the aircraft, it is possible to construct reference trajectories for a six-degree-of-freedom aircraft by transforming the velocity vector from the inertial frame to the aircraft body frame and differentiating the direction cosines to obtain the required aircraft angular velocities. A straightforward inversion yields the required aircraft control surface deflections. The approach enables sampling times on the order of 1 s using the basic algorithm implemented on a laptop computer running MATLAB. Closed-loop simulations show good tracking of the reference trajectories and safe maneuvering near three-dimensional

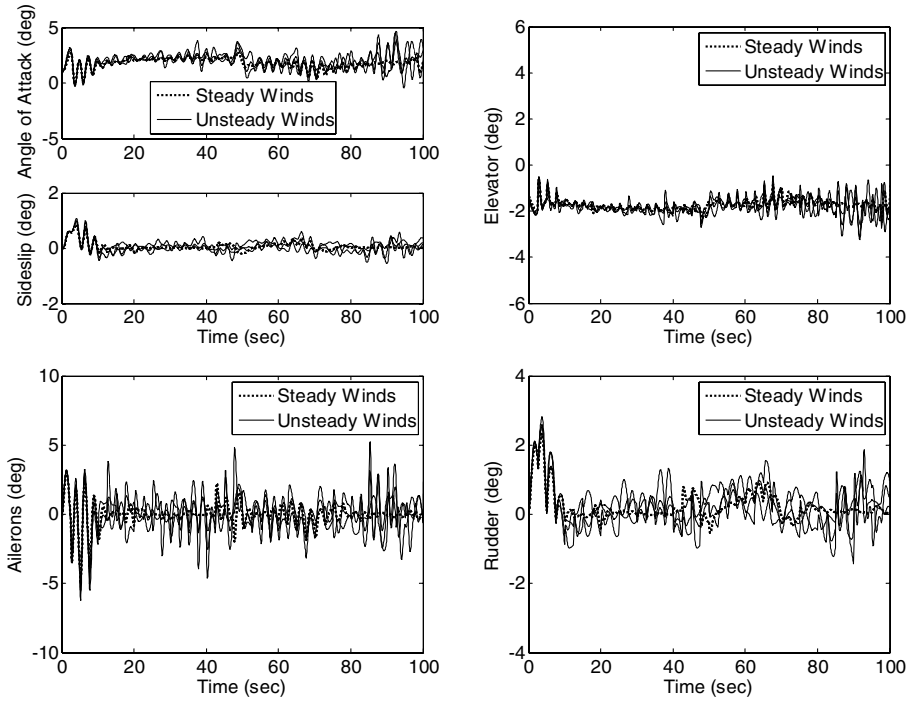

Fig. 2 Example results from Monte Carlo simulations.

terrain in the presence of unsteady external disturbances. The inner-loop tracking controller plays an important role in the dynamics, both in terms of the accuracy of the tracking and the speed with which the outer loop can be updated. Further work should be undertaken to improve the design of inner loops to account for the discontinuous accelerations and moments that are often required across an outer-loop update.

References

[1] Barfield, F., Probert, J., and Browning, D., "All Terrain Ground Collision Avoidance and Maneuvering Terrain Following for Automated Low-Level Night Attack," *IEEE Aerospace and Electronic Systems Magazine*, Vol. 8, No. 3, March 1993, pp. 40–47.

[2] Menon, P. K. A., Kim, E., and Cheng, V. H. L., "Optimal Trajectory Synthesis for Terrain-Following Flight," *Journal of Guidance, Control, and Dynamics*, Vol. 14, No. 4, 1991, pp. 807–813.

[3] Twigg, S., Calise, A., and Johnson, E., "On-Line Trajectory Optimization Including Moving Threats and Targets," AIAA Paper 2004-5139, Aug. 2004.

[4] Richards, A., and How, J. P., "Aircraft Trajectory Planning with Collision Avoidance Using Mixed Integer Linear Programming," *Proceedings of the American Control Conference, Anchorage, AK*, Institute of Electrical and Electronics Engineers, Piscataway, NJ, May 2002, pp. 1936–1941.

[5] Xu, Z., Yunan, H., and Pingyuan, C., "Study of Terrain Following Controller Based on Backstepping and Variable Structure Control," *Proceedings of the 5th World Congress on Intelligent Control and Automation, Hangzhou, China*, Institute of Electrical and Electronics Engineers, Piscataway, NJ, June 2004, pp. 5475–5478.

[6] Funk, J. E., "Optimal-Path Precision Terrain-Following System," *Journal of Aircraft*, Vol. 14, No. 2, 1977, pp. 128–134.

[7] Asseo, S. J., "Terrain Following/Terrain Avoidance Path Optimization using the Method of Steepest Descent," *Proceedings of the IEEE National Aerospace and Electronics Conference*, Vol. 3, Inst. of Electrical and Electronics Engineers, New York, 1988, pp. 1128–1136.

[8] Lu, P., and Pierson, B. L., "Optimal Aircraft Terrain-Following Analysis and Trajectory Generation," *Journal of Guidance, Control, and Dynamics*, Vol. 18, No. 3, 1995, pp. 555–560.

[9] Lu, P., and Pierson, B. L., "Aircraft Terrain Following Based on a Nonlinear Continuous Predictive Control Approach," *Journal of Guidance, Control, and Dynamics*, Vol. 18, No. 4, 1995, pp. 817–823.

[10] Williams, P., "Aircraft Trajectory Planning for Three-Dimensional Terrain Following Incorporating Actuator Constraints," *Journal of Aircraft*, Vol. 42, No. 5, 2005, pp. 1358–1362.

[11] Sharma, T., Williams, P., Bil, C., and Eberhard, A., "Optimal Three-Dimensional Aircraft Terrain Following and Collision Avoidance," *The 7th Biennial Engineering Mathematics and Applications Conference, Melbourne, Australia, Sept. 25–28, 2005*, Royal Melbourne Institute of Technology, Melbourne, Australia, 2005.

[12] Menon, P. K., Sweriduk, G. D., and Sridhar, B., "Optimal Strategies for Free-Flight Air Traffic Conflict Resolution," *Journal of Guidance, Control, and Dynamics*, Vol. 22, No. 2, 1999, pp. 202–211.

[13] Bryson, A. E., Desai, M. N., and Hoffman, W. C., "Energy-State Approximation in Performance Estimation of Supersonic Aircraft," *Journal of Aircraft*, Vol. 6, No. 6, 1969, pp. 481–487.

[14] Bryson, A. E., *Dynamic Optimization*, Addison–Wesley, Menlow Park, CA, 1999, pp. 172–176.

[15] Stengel, R. F., *Flight Dynamics*, Princeton Univ. Press, Princeton, NJ, 2004, p. 47.

[16] Williams, P., "Real-Time Computation of Optimal Three-Dimensional Aircraft Trajectories including Terrain-Following," AIAA Paper 2006-6603, 2006.

[17] Elnagar, G., Kazemi, M. A., and Razzaghi, M., "Pseudospectral Legendre Method for Discretizing Optimal Control Problems," *IEEE Transactions on Automatic Control*, Vol. 40, No. 10, 1995, pp. 1793–1796.

[18] Ross, I. M., and Fahroo, F., *Legendre Pseudospectral Approximations of Optimal Control Problems*, Lecture Notes in Control and Information Sciences, Vol. 295, Springer–Verlag, Berlin, 2003, pp. 327–342.

[19] Gill, P. E., Murray, W., and Saunders, M. A., "SNOPT: an SQP Algorithm for Large-Scale Constrained Optimization," *SIAM Journal on Optimization*, Vol. 12, No. 4, 2002, pp. 979–1006.

[20] Yan, H., Fahroo, F., and Ross, I. M., "Real-Time Computation of Neighbouring Optimal Control Laws," *AIAA Guidance, Navigation, and Control Conference*, AIAA Paper 2002-4657, 2002.

[21] Williams, P., "Receding Horizon Control Using Gauss–Lobatto Quadrature Approximations," *AAS/AIAA Astrodynamics Specialist Conference*, American Astronautical Society Paper 05-349, 2005.